

Optical-lattice based Cs active clock with continual superradiant lasing signal

¹Duo Pan, ²Bindiya Arora, ³Yan-mei Yu,* ⁴B. K. Sahoo,† and ¹Jingbiao Chen‡

¹State Key Laboratory of Advanced Optical Communication Systems and Networks,
Department of Electronics, Peking University, Beijing 100871, China

²Department of Physics, Guru Nanak Dev University, Amritsar, Punjab 143005, India

³Beijing National Laboratory for Condensed Matter Physics,
Institute of Physics, Chinese Academy of Sciences, Beijing 100190, China and

⁴Atomic, Molecular and Optical Physics Division,
Physical Research Laboratory, Navrangpura, Ahmedabad 380009, India

(Dated: August 27, 2020)

We demonstrate state-of-the-art technique of an active clock to provide a continuous superradiant lasing signal using an ensemble of trapped Cs atoms in the optical lattice. A magic wavelength of the proposed $|7S_{1/2}; F = 4, M_F = 0\rangle \rightarrow |6P_{3/2}; F = 3, M_F = 0\rangle$ clock transition in Cs atom is identified at 1181 nm for constructing the optical lattice. Pertinent optical lines are also found for pumping and repumping atoms from their ground states. A fractional uncertainty about 10^{-15} level to the clock frequency has been predicted by carrying out rigorous calculations of several atomic properties. The bad-cavity operational mode of the active clock is anticipated to improve its short-term stability remarkably by suppressing intrinsic thermal fluctuations. Thus, a composite clock system with better in both short-term and long-term stabilities can be built by combining the above proposed active clock with another high-accuracy passive optical clock.

It is well known that owing to its natural immunity against the cavity thermal noise floor, hydrogen masers offer better instability among the microwave atomic clocks within the first 30 seconds of frequency measurement, referred to as its short-term stability. On the other hand, the short-term stabilities of the existing high-precision optical passive clocks have strict requirement for are constrained by the thermal noise of the local oscillators' super-cavities instabilities of the local oscillators and the thermal noise floor of reference cavities. With the development of cryogenic optical cavities thermal noise has been continuously reduced [1–3], and the short-term instability of local oscillators as low as $4\text{E-}17@1\text{s}$ has been achieved. This has brought significant improvement in the short-term stability of passive optical clocks [4–9]. In the meantime, a new direction has emanated to improve short-term stability for an optical clock. By manifesting the working principle of hydrogen maser, building an active optical clock is steadily gaining the ground [10–15]. The underlying principle of an active optical clock lies in its robustness to infer the clock frequency directly from the superradiant signal of an ensemble of atoms placed inside a “bad-cavity”. In principle, the active optical clock can achieve short-term instabilities well below the cavities thermal noise limit and at the same time it can relax the requirement for the cryogenic ultra-stable cavity, thus reducing the systematic complexity. The short-term stabilities of these clocks can be improved appreciably by suppressing photon shot-noises through continuous pumping and output lasing signals. The previously proposed two-level active optical clocks [13, 14] are compelled to produce signals intermittently to overcome interference between the applied pumping pulse with the output clock lasing signal. The stability and accuracy of a continuously signal pro-

ducing proposed in three-level clock [10] are critically obstructed by the light shift caused by the pumping laser. To explore in this direction further, we had analyzed four atomic levels accessible by optical lasers in an ensemble of thermal Cs atoms for a possible continuously signal producing active optical clock in Ref. [16]. However, this is also subjected to large systematics due to light shifts and collisional decoherence.

In this Letter, we expound feasibility of an active optical clock using four suitable hyperfine levels of trapped cold Cs atoms, instead of atomic energy levels of thermal Cs atoms proposed in Ref. [16], in a red-detuned one-dimensional (1D) optical lattice at a magic wavelength (λ_m) of the $|7S_{1/2}; F = 4, M_F = 0\rangle \rightarrow |6P_{3/2}; F = 3, M_F = 0\rangle$ clock transition. The schematic layout of our experimental set-up and the associated hyperfine levels are shown in Figs. 1(a) and (b), respectively. The unique advantages of adopting this technique with appropriate choices of hyperfine levels are at least three folds over the previous active optical clocks, such as it moderates interference between the pumping laser and the superradiant lasing signal, and minimizes light shifts and collisional decoherence to the hyperfine levels and provides sufficient time to conduct the experiment meticulously due to strong confinements of atoms in the optical lattice. A sufficiently weak magnetic field, of about $\mathcal{B} = 10^{-7}$ T, is applied to break the M_F degeneracy of the clock transition and a π -polarized pumping laser is locked at 455 nm for populating Cs atoms to the $|7P_{3/2}; F = 5, M_F = 0\rangle$ level from the $|6S_{1/2}; F = 4, M_F = 0\rangle$ level of the ground state. Subsequently, these atoms decay to any of the $M_F = -1, 0$, or 1 sublevels of the $F = 4$ hyperfine level of the $7S_{1/2}$ state through spontaneous emission. At the same time, a mode of bad-cavity is adjusted to couple with the clock transition, which is further locked to a

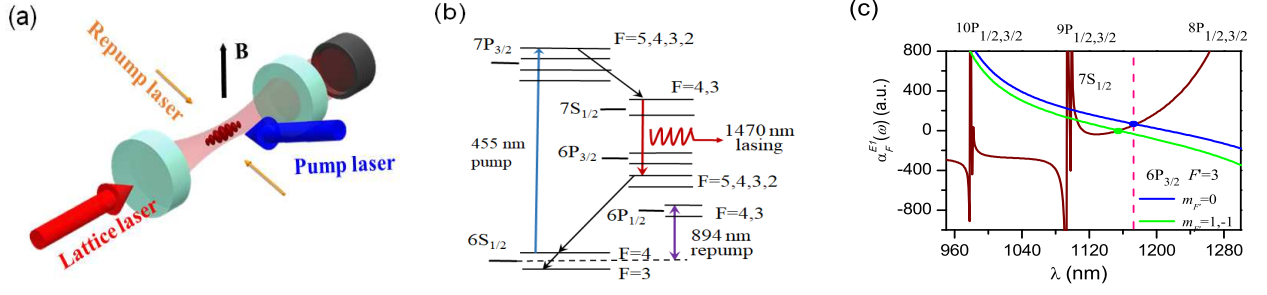


FIG. 1. Schematic depictions of (a) experimental set-up, in which cold Cs atoms are held in an 1D optical lattice situated inside a high finesse cavity near magic wavelength (λ_m) of $|7S_{1/2}; F=4, M_F=0\rangle \rightarrow |6P_{3/2}; F=3, M_F=0\rangle$ clock transition of the proposed four-level active clock, (b) the relevant energy levels for clock, pumping and repumping transitions, and (c) plot for $\alpha_F^{E1}(\omega)$ values (in a.u.) of the clock levels against wavelength λ (in nm) to infer required λ_m . Resonance lines for the $7S_{1/2}$ state are marked on the top of plot.

super-cavity [16]. The objective of this step is to attain self-gaining stimulated emission from the above transition in the bad-cavity mode and produce a superradiant lasing. A polarization selector inside the cavity (not shown in the figure) helps to establish a superradiant lasing signal in the above transition through the allowed ($M_F \rightarrow M_F$) $\equiv (0 \rightarrow 0)$, $(1 \rightarrow 1)$, and $(-1 \rightarrow -1)$ decay channels. Then, atoms come down to either of the $F=3$ or $F=4$ hyperfine levels of the ground state. A 894 nm laser is applied at this stage to re-pump the atoms from all other magnetic sub-levels to the desired $|6S_{1/2}; F=4, M_F=0\rangle$ level of the ground state by using a dual-laser [17]. The combined pumping action, spontaneous emission, superradiant emission, and spontaneous decay channels follow the path of the $6S_{1/2} \rightarrow 7P_{3/2} \rightarrow 7S_{1/2} \rightarrow 6P_{3/2} \rightarrow 6S_{1/2}$ transitions successively to populate the $|6S_{1/2}; F=4, M_F=0\rangle$ level in the end of a complete cycle to perpetuate a continuous loop of clock operation. There is a probability that a fraction of atoms can populate in the $5D_{3/2,5/2}$ states through spontaneous emission from the $7P_{3/2}$ state, but they will decay to the $6P_{1/2,3/2}$ states within 0.1 μ s. Thus, the superradiant lasing is not going to be affected by such process. Since interferences between the (re)pumping laser and the clock lasing signal do not occur in this procedure, a continuous signal of superradiant lasing at 1470 nm can be achieved.

An essential feature of our proposed experimental technique is to trap Cs atoms at a λ_m of the clock transition in an optical lattice. The most convenient choice is to use a π -polarized laser for creating trapping potential, which can cause the ac-Stark shift in a hyperfine $|F, M_F\rangle$ level of atomic state as $\Delta E_F(\omega) = -\frac{1}{4}\alpha_F^{E1}(\omega)\mathcal{E}^2$ with amplitude of electric field \mathcal{E} of trapping laser and dynamic electric dipole (E1) polarizability of hyperfine level $\alpha_F^{E1}(\omega)$ for laser frequency ω . The $\alpha_F^{E1}(\omega)$ values of the hyperfine levels of the $7S_{1/2}$ and $6P_{3/2}$ clock states are determined by calculating their atomic-state polarizability $\alpha_J^{E1}(\omega)$ values using the same method as in Refs. [18, 19]. For

this purpose, we have used the experimental energies and E1 matrix elements either from the literature [20–22] or by calculating them using a relativistic all-order method [23]. Uncertainties to the α_F^{E1} values are determined from the accuracies of the E1 matrix elements. The λ_m values of a transition corresponds to its null differential $\alpha_F^{E1}(\omega)$ values. We plot the $\alpha_F^{E1}(\omega)$ values of the hyperfine levels of the $7S_{1/2}$ and $6P_{3/2}$ states in Fig. 1(c) for the optical range of 950 – 1300 nm to locate possible λ_m values. The intersections of the polarizability curves mark the presence of a suitable λ_m at 1181 nm. The inferred $\alpha_F^{E1}(\omega)$ values of different states at $\lambda_m = 1181$ nm are quoted in atomic units (a.u.) in Table I. At 1181 nm, α_F^{E1} is 73(10) a.u. for the $7S_{1/2}, F=4$ upper clock state, and $\alpha_F^{E1} = 73(36)$ a.u. for the $6P_{3/2}, F=3$ lower clock state, as determined by its scalar and tensor α_J^{E1} values of -381(32) a.u. and 629(13) a.u., respectively.

The 455 nm pumping laser can populate Cs atoms from the ground state on the excited state, simultaneously, the 894 nm repumping laser is used for Sisyphus cooling. The temperature of the trapped cold Cs atoms is determined by balancing the heating rate and the cooling effect; $k_B T_c = (D_p + D'_p)/\alpha_{cool}$, where D_p and D'_p are the momentum diffusion coefficients of the pumping and repumping lasers, respectively, and α_{cool} is the cooling coefficient due to the 894 nm laser. It yields $D_p = \frac{1}{2}\hbar^2 k^2 \Gamma_{455} = 1.9 \times 10^{-48} \text{kg}^2 \text{m}^2 / \text{s}^3$ [24] with the Rabi frequency $\gg \Gamma_{455}$, wherein k and Γ_{455} are the wave vector and spontaneous decay rate, respectively, of the pumping transition and \hbar is the Planck constant. We estimate $D'_p = 9.1 \times 10^{-48} \text{kg}^2 \text{m}^2 / \text{s}^3$ for a repumping laser intensity of 2 mW/cm² and detuning $\delta = 30$ MHz using the formula $D'_p = (7/10)\hbar^2 k'^2 \Gamma_{894} s_0 + (3/4)\hbar^2 k'^2 (\delta^2 / \Gamma_{894}) s_0$ [25, 26], where $s_0 = \frac{\Omega^2/2}{\delta^2 + \Gamma_{894}^2/4}$ is saturation parameter, wave vector k' , Rabi frequency Ω and spontaneous decay rate Γ_{894} of the repumping transition. Similarly, $\alpha_{cool} = 29\hbar^2 k'^2 \Gamma_{894} / (50k_B T_0) = 2.2 \times 10^{-20} \text{kg/s}$ is obtained using the reported Sisyphus cooling tempera-

TABLE I. Properties of Cs atoms and optical trap at 1181 nm magic wavelength. Here, τ , α_J^{E1} and ρ represent natural lifetimes, atomic dipole polarizabilities, and populations, respectively, of investigated states in Cs atom, while U_0 , Γ_{sc} and τ_L correspond to trapping potential, scattering rate and lifetimes of atomic states due to the scattered photons, respectively, in the 1D optical lattice for the operational laser intensity $I_{op} = 20 \text{ kW/cm}^2$. Uncertainties to the α_J^{E1} values are quoted explicitly, which are used for estimating the clock frequency shift.

State	$\tau(\mu\text{s})$	$\alpha_J^{E1}(\text{a.u.})$	$U_0(\text{kHz})$	$\rho(\%)$	$\Gamma_{sc}(\text{kHz/s})$	$\tau_L(\text{s})$
$6S_{1/2}$	∞	846(11)	-2957	27.1	2.6	1137
$5D_{5/2}$	1.37	793(38)	-2772	33.9	21.5	129
$5D_{3/2}$	0.97	730(37)	-2551	3.1	13.0	196
$7P_{3/2}$	0.11	8045(4388)	-28119	24.1	0.1	$> 10^5$
$7S_{1/2}$	0.05	73(10)	-255	5.5	0.3	850
$6P_{3/2}$	0.03	-381(32)	-255	2.7	6.8	38

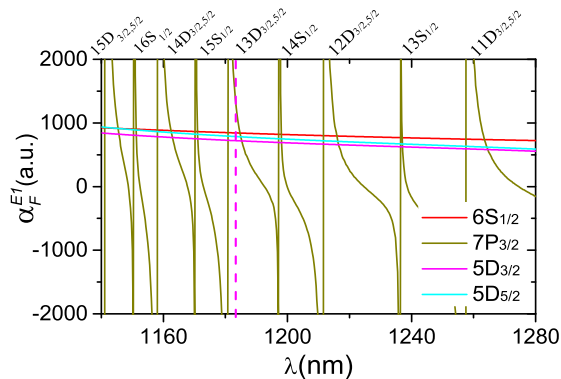


FIG. 2. Plot for $\alpha_F^{E1}(\omega)$ values (in a.u.) of hyperfine levels used for pumping and repumping transitions against wavelength (in nm). Resonance lines of the $7P_{3/2}$ state are labeled on the top of plot. The dashed line shows the position of the λ_m value (i.e. 1181 nm) for the optical lattice.

ture $T_0 = 30 \mu\text{K}$ [27]. Accounting for the above parameters, it yields the cooling temperature of the system $T_c = 35 \mu\text{K}$, which is low enough to ensure effective loading of Cs atoms into the lattice.

The dipole potential of the 1D red-detuned optical lattice is constructed following Ref. [28]. The maximum trapping depth at the antinode position of the lattice is determined by $U_0 = -\alpha_F^{E1}(\omega)\mathcal{E}^2$ with $\mathcal{E} = \sqrt{2I/(c\epsilon_0)}$, where c and ϵ_0 are speed of light and vacuum permittivity, respectively, and I is average intensity of laser. The strength of the trapping potential is gauged by investigating the $\alpha_F^{E1}(\omega)$ values for the corresponding hyperfine levels of the considered states at $\lambda_m = 1181 \text{ nm}$. The $\alpha_F^{E1}(\omega)$ values of the levels associated with the pumping and repumping transitions are plotted for the wavelength range from 1140 nm to 1280 nm in Fig. 2. Using the $\alpha_F^{E1}(\omega)$ values, calculated in the same procedure as in Refs. [18, 19], it gives U_0 for the $6S_{1/2}$ and $5D_{3/2,5/2}$ states, using a typical operational lattice intensity $I_{op} = 20 \text{ kW/cm}^2$, three times larger than the thermal kinetic energy $k_B T$ of the trapped atoms at the estimated temperature $T \sim 35 \mu\text{K}$ and Boltzmann con-

stant k_B . Due to presence of a large number of resonant lines, it was strenuous to predict definite signs of $\alpha_F^{E1}(\omega)$ of the $7P_{3/2}$ state around $\lambda_m = 1181 \text{ nm}$. Also, the U_0 values for the $7S_{1/2}$ and $6P_{3/2}$ states turn out to be quite small. Nonetheless, atoms will decay from these states to the $6S_{1/2}$ and $5D_{3/2,5/2}$ states within tens of nanoseconds before they could escape from the lattice.

Since it is imperative to operate the optical lattice at a very low sensitivity against variation in the trapping laser wavelength to minimize fluctuation in the clock frequency, we estimate the rate of change in the clock frequency with respect to deviation in wavelength per unit power of the trapping laser. This comes out to be of the order of $0.7 \text{ Hz}/(\text{GHz}\cdot\text{kW/cm}^2)$ around $\lambda_m = 1181 \text{ nm}$ from Fig. 1(c). By assuming a typical experimental condition of maximum 100 kHz deviation in the trapping laser frequency [29], the fractional clock frequency shift is expected to be about 6.9×10^{-18} for a typical value of $I_{op} = 20 \text{ kW/cm}^2$.

The steady-state atomic populations in the investigated four levels of Cs atom during the clock frequency measurement are obtained by considering atom-pumping laser interactions in the Liouville or von Neumann equation, given by [30]

$$\frac{d\rho}{dt} = \frac{1}{i\hbar} [H_{AP}, \rho] - \frac{1}{2} \{\Gamma, \rho\}, \quad (1)$$

where $H_{AP} = H_{AP}^0 + H_{AP}^I$ is the total Hamiltonian comprising of the unperturbed Hamiltonian describing the upper ($|F_u, M_{F_u}\rangle$) and the lower ($|F_l, M_{F_l}\rangle$) levels of the pumping (or repumping) transition as $H_{AP}^0 = \sum_{i=u,l} E_{F_i} |F_i, M_{F_i}\rangle \langle F_i, M_{F_i}|$ with the eigenvalues E_{F_i} in the absence of laser field and interaction Hamiltonian $H_{AP}^I = -\frac{i}{\hbar} [\Omega_{F_l F_u} |F_l, M_{F_l}\rangle \langle F_u, M_{F_u}| + \Omega_{F_u F_l} |F_u, M_{F_u}\rangle \langle F_l, M_{F_l}|]$ with the Rabi frequencies $\Omega_{F_l F_u} = \Omega_{F_u F_l} = |\langle F_l || D || F_u \rangle| \mathcal{E} / \hbar$ for the field strength \mathcal{E} . We have used experimental values of energies and transition rates [31, 32] to predict the atomic populations, which are shown in Fig. 3 for all the hyperfine levels of the above states and quoted explicitly in Table I by taking the

pumping and repumping powers 500 mW/cm² and 2 mW/cm², respectively.

We also present the estimated lifetime τ_L and photon scattering rate Γ_{sc} values in Table I. The lifetime of an atomic state in the far-detuned optical lattice trap due to photon scattering is estimated by $\tau_L = U_0/\Gamma_{sc}$, and the photon scattering rate Γ_{sc} can be formulated as

$$\Gamma_{sc} = \frac{1}{6(2J_n + 1)} \sum_k \frac{|\langle J_n || D || J_k \rangle|^2}{(\hbar\omega_L - \delta E_{nk})^2} \Gamma_k \mathcal{E}^2, \quad (2)$$

where Γ_k is spontaneous decay rate from upper state k to lower state n , and ω_L is lattice laser frequency. As can be seen, the τ_L values are at least a few tens of seconds for different states, among which the $6P_{3/2}$ state has the shortest lifetime. This is still long enough for continuous operation of the clock.

The output power of the superradiant laser in the atom-cavity coupled system is determined by solving the Born-Markov master equation [10, 11], given by

$$\frac{d\rho}{dt} = \frac{1}{i\hbar} [H_{AC}, \rho] + \mathcal{L}[\rho], \quad (3)$$

for upper $|F_u, M_{F_u}\rangle$ and lower $|F_l, M_{F_l}\rangle$ levels of the clock transition. Here, the total Hamiltonian of the system is given by $H_{AC} = H_{AC}^0 + H_{AC}^I$ with the unperturbed

Hamiltonian $H_{AC}^0 = \left[\sum_{j=1}^{N_a} \frac{\hbar\omega_a}{2} \hat{\sigma}_j^z + \hbar\omega_c \hat{a}_c^\dagger \hat{a}_c \right]$ and the in-

teraction Hamiltonian $H_{AC}^I = \frac{\hbar g}{2} \sum_{j=1}^{N_a} (\hat{a}_c^\dagger \hat{\sigma}_j^- + \hat{a}_c \hat{\sigma}_j^+)$.

In these expressions, ω_a is the angular frequency of the clock transition, ω_c is the angular frequency of the cavity mode, $\hat{\sigma}_j^z = |F_u^j, M_{F_u}^j\rangle\langle F_u^j, M_{F_u}^j| - |F_l^j, M_{F_l}^j\rangle\langle F_l^j, M_{F_l}^j|$, $\hat{\sigma}_j^- = (\hat{\sigma}_j^+)^{\dagger} = |F_u^j, M_{F_u}^j\rangle\langle F_l^j, M_{F_l}^j|$, atom-cavity coupling constant $g = \mu\sqrt{\frac{8\pi\omega_a}{\hbar\epsilon_0 V_c}} = 4.09 \times 10^6$ Hz for the actual E1 matrix element μ of the clock transition and cavity mode volume V_c , and $\mathcal{L}[\rho]$ is the net Liouvillian containing contributions from the cavity, spontaneous decay, pumping laser and inhomogeneous lifetime of the upper state. The output power of the bad-cavity is estimated as $P = \hbar\omega_a \kappa |\text{tr}[\rho_{cw} a_c]|^2$ for the steady-state solution ρ_{cw} of the above equation and cavity dissipation rate κ . The estimated steady-state output power of the superradiant lasing is $P = 24 \mu\text{W}$ for a typical $N_a = 10^7$ number of atoms achieved through population-inversion with the pumping and repumping laser intensities of 500 mW/cm² and 2 mW/cm², respectively.

The quantum restricted linewidth $\Delta\nu$, following the modified Schawlow-Townes formula for bad-cavity, is given by [12]

$$\Delta\nu = \frac{\hbar\omega_a \kappa^2}{4\pi P} N_{sp} \left(1 + \left[\frac{2(\omega_c - \omega_a)}{\Gamma_u + \kappa} \right]^2 \right) \left(\frac{\Gamma_u}{\Gamma_u + \kappa} \right)^2, \quad (4)$$

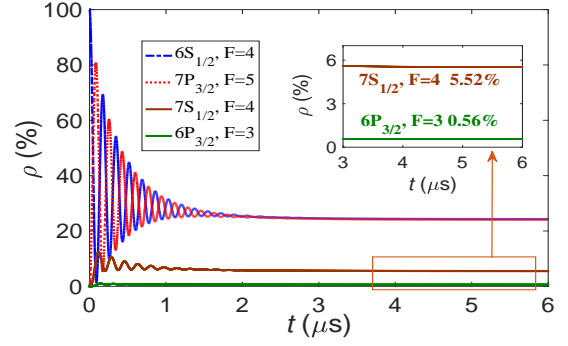


FIG. 3. Steady-state atomic populations ρ (in %) in different levels over a range of time scale t (in μs). Lattice, pumping, and repumping lasers are π -polarized, and the lattice laser is adjusted to be resonating with a mode of cavity.

TABLE II. Scalar and tensor components of E1 polarizabilities (in a.u.), and M1 polarizabilities (in a.u.) of the clock levels. Estimated fractional shifts to the clock frequency from various systematics using the above quantities are listed in the bottom part.

Properties	$ 7S_{1/2}(F=4)\rangle$	$ 6P_{3/2}(F=3)\rangle$
$\alpha_F^{E1(0)}(0)$	6238(15)	1647(35)
$\alpha_F^{E1(0)}(455\text{nm})$	82(3)	-54(24)
$\alpha_F^{E1(0)}(894\text{nm})$	-267(11)	-4129(111)
$\alpha_F^{E1(2)}(455\text{nm})$	0	-3(1)
$\alpha_F^{E1(2)}(894\text{nm})$	0	1679(25)
α_F^{M1}	$-1.4(1) \times 10^4$	$-2.6(2) \times 10^5$
Fractional frequency shifts		
BBR static at 300K	$1.94(2) \times 10^{-13}$	
455nm laser, $I=500\text{mW/cm}^2$	$-1.6(7) \times 10^{-14}$	
894nm laser, $I=2\text{mW/cm}^2$	$-1.8(1) \times 10^{-15}$	
2^{nd} -Zeeman, $\mathcal{B}=10^{-7}$ T	$-7.1(3) \times 10^{-19}$	

where $N_{sp} = \rho_u/(\rho_u - \rho_l)$ with ρ_u and ρ_l being atomic population densities in upper and lower states, and Γ_u is the spontaneous decay rate of the clock transition. We have set the cavity dissipation rate as $\kappa = 100 \Gamma_u$. The quantum-limit linewidth of the superradiant lasing is anticipated to be narrowed down to 4.2 mHz for the 5.5% and 0.6% population densities in the upper and lower levels of the clock transition, respectively.

Typical orders of magnitudes of the major systematics to the clock frequency due to black-body radiation (BBR) shifts, light shifts caused by the pumping and repumping lasers, and the second-order Zeeman shifts, are determined by using the scalar ($\alpha_F^{E1(0)}$) and tensor ($\alpha_F^{E1(2)}$) E1 polarizabilities and magnetic dipole (M1) polarizabilities (α_F^{M1}) of the hyperfine levels that are listed in Table II. Using the differential static scalar E1 polarizabilities, $\delta\alpha_F^{E1(0)}(0)$ between the $|7S_{1/2}; F=4, M_F=0\rangle$ and $|6P_{3/2}; F=3, M_F=0\rangle$ clock levels, the BBR shift

at the room temperature (300 K) is determined by

$$\delta E_{\text{BBR}}^{\text{E1}} = -\frac{1}{2}(831.9 \text{ V/m})^2 \left[\frac{T(\text{K})}{300} \right]^4 \delta \alpha_F^{\text{E1}(0)}(0). \quad (5)$$

The fractional BBR shift in the clock frequency is estimated to be $1.94(2) \times 10^{-13}$. This uncertainty can be suppressed by two more orders by measuring the differential scalar E1 polarizability of the clock transition more precisely and conducting the experiment at a lower temperature. The light shifts due to the pumping and repumping lasers lead to the fractional clock frequency shifts $-1.6(7) \times 10^{-14}$ and $-1.8(1) \times 10^{-15}$, respectively. Since powers of these lasers can be controlled with an instability below 10^{-4} [33, 34], it is possible to curtail the above fractional uncertainties to the 10^{-18} level. The choice of the $M_F = 0 \rightarrow M_F = 0$ clock transition gives zero first-order Zeeman shift. The second-order Zeeman shift of a hyperfine level is estimated by $\Delta E_{\text{Zeem}}^{2nd} = -\frac{1}{2} \alpha_F^{\text{M1}} \mathcal{B}^2$. The fractional shift in the clock frequency due to this effect is estimated from the difference of α_F^{M1} values, which is determined as $\alpha_F^{\text{M1}} = -\frac{2}{3(2F+1)} \sum_i \frac{|\langle F || O^{\text{M1}} || F_i \rangle|^2}{E_F - E_{F_i}}$ for M1 operator O^{M1} and all possible F_i levels of the clock states with energies E_{F_i} . Uncertainties to these quantities come mainly from the energies. The α_F^{M1} values of the $|7S_{1/2}; F=4, M_F=0\rangle$ and $|6P_{3/2}; F=3, M_F=0\rangle$ levels are found to be -1.4×10^4 a.u. and -2.6×10^5 a.u., respectively. This gives a negligibly small fractional second-order Zeeman shift to the clock frequency. Other systematic effects are expected to be much lower than 10^{-15} level.

In summary, we have proposed a continual superradiant lasing scheme to construct an active lattice clock based on optical lattices. A suitable magic wavelength of the $|7S_{1/2}; F=4, M_F=0\rangle \rightarrow |6P_{3/2}; F=3, M_F=0\rangle$ clock transition of Cs atom has been narrowed down to confine atoms strongly in the optical lattices with densely populated ground and excited states. By simulating realistic experimental conditions, we predict to achieve fractional uncertainty to the clock frequency about 10^{-15} level and linewidth of a few mHz. Its bad-cavity operational mode can provide a robust short-term stability to this active clock. This in combination with another high-accuracy passive optical clock can be used to cater better short-term and long-term stabilities for practical applications.

The work was supported by National Natural Science Foundation of China (NSFC) (91436210, 11874064) and the Strategic Priority Research Program of the Chinese Academy of Sciences (CAS), Grant No. XDB21030300, and the NKRD Program of China, Grant No. 2016YFA0302104. The work of B.A. is supported by DST-SERB (India) Grant No. EMR/2016/001228. B.K.S. thanks IOP, Beijing for the overseas professor fellowship and hospitality to carry out this work. D.P and J.B.C acknowledge valuable discussions with F. Fang.

* ymyu@aphy.iphy.ac.cn

† bijaya@prl.res.in

‡ jbchen@pku.edu.cn

- [1] D. G. Matei, T. Legero, S. Häfner, C. Grebing, R. Weyrich, W. Zhang, L. Sonderhouse, J. M. Robinson, J. Ye, F. Riehle, and U. Sterr, *Phys. Rev. Lett.* **118**, 263202 (2017).
- [2] T. Kessler, C. Hagemann, C. Grebing, T. Legero, U. Sterr, F. Riehle, M. J. Martin, L. Chen, and J. Ye, *Nature Photon.* **6**, 687 (2011).
- [3] W. Zhang, J. M. Robinson, L. Sonderhouse, E. Oelker, C. Benko, J. L. Hall, T. Legero, D. G. Matei, F. Riehle, U. Sterr, and J. Ye, *Phys. Rev. Lett.* **119**, 243601 (2017).
- [4] T. L. Nicholson, S. L. Campbell, R. B. Hutson, G. E. Marti, B. J. Bloom, R. L. McNally, W. Zhang, M. D. Barrett, M. S. Safronova, G. F. Strouse, W. L. Tew, and J. Ye, *Nat. Commun.* **6**, 6896 (2015).
- [5] R. Yanagimoto, N. Nemitz, F. Bregolin, and H. Katori, *Phys. Rev. A* **98**, 012704 (2018).
- [6] J. S. Chen, S. M. Brewer, C. W. Chou, D. J. Wineland, D. R. Leibbrandt, and D. B. Hume, *Phys. Rev. Lett.* **118**, 053002 (2017).
- [7] N. Huntemann, C. Sanner, B. Lipphardt, Chr. Tamm, and E. Peik, *Nature* **116**, 063001 (2016).
- [8] A. Golovizin, E. Fedorova, D. Tregubov, D. Sukachev, K. Khabarova, V. Sorokin, and N. Kolachevsky, *Nat. Commun.* **10**, 1074 (2019).
- [9] S. Sonar, M. Hajdusek, M. Mukherjee, R. Fazio, V. Vedral, S. Vinjanampathy, and L.C. Kwek, *Phys. Rev. Lett.* **120** 163601 (2018).
- [10] D. Meiser, J. Ye, D. R. Carlson, and M. J. Holland, *Phys. Rev. Lett.* **102**, 163601 (2009).
- [11] G. A. Kazakov and T. Schumm, *Phys. Rev. A* **95**, 023839, (2017).
- [12] S. J. M. Kuppens, M. P. van Exter, and J. P. Woerdman, *Phys. Rev. Lett.* **72** 3815 (1994).
- [13] M. A. Norcia, J. R. K. Cline, J. A. Muniz, J. M. Robinson, R. B. Hutson, A. Goban, G. E. Marti, J. Ye, and J. K. Thompson, *Phys. Rev. X* **8**, 021036 (2018).
- [14] T. Laske, H. Winter, and A. Hemmerich, *Phys. Rev. Lett.* **123**, 103601 (2019).
- [15] D. Yu and J. Chen, *Phys. Rev. Lett.* **98**, 050801 (2007).
- [16] D. Pan, T. Shi, and J. Chen, *IEEE T. Ultrason. Ferr.* **65**, 1958 (2018).
- [17] G. Avila, E. Clercq, M. Labachellerie, and P. Cézé, *IEEE T. Instrum. Meas.* **34**, 139 (1985).
- [18] S. Singh, B. K. Sahoo, and B. Arora, *Phys. Rev. A* **93**, 063422 (2016).
- [19] S. Singh, K. Kiranpreet, B. K. Sahoo, and B. Arora, *J. Phys. B: At. Mol. Opt. Phys.* **49**, 145005 (2016).
- [20] G. Toh, A. Damitz, C. E. Tanner, W. R. Johnson, and D. S. Elliott, *Phys. Rev. Lett.* **123** 073002 (2019).
- [21] A. Damitz, G. Toh, E. Putney, C. E. Tanner, and D. S. Elliott, *Phys. Rev. A* **99**, 062510 (2019).
- [22] G. Toh, A. Damitz, N. Glotzbach, J. Quirk, I. C. Stevenson, J. Choi, M. S. Safronova, and D. S. Elliott, *Phys. Rev. A* **99**, 032504 (2019).
- [23] M.S. Safronova and W.R. Johnson, *Advances In Atomic, Molecular, and Optical Physics* **55** 191 (2008).
- [24] P. Lett, W. Phillips, and S. Rolston, *J. Opt. Soc. Am. B* **6**, 2084 (1989).

- [25] J. Dalibard and C. Cohen-tannoudji, *J. Opt. Soc. Am. B* **6**, 2023 (1989).
- [26] J. Dalibard, S. Reynaud, and C. Cohen-tannoudji, *J. Phys. B: At. and Mol. Phys.* **17**, 4577 (1984).
- [27] J. Hou, Y. Li, D. Yang, and Y. Wang, *Acta Phys. Sinica* **7**, 881 (1998).
- [28] A. Derevianko and H. Katori, *Rev. Mod. Phys.* **83**, 331 (2011).
- [29] M. M. Boyd, Ph.D Thesis, University of Colorado (2007).
- [30] M. O. Scully and M. S. Zubairy, *Quantum optics*, Cambridge university press, UK, (1997).
- [31] D. A. Steck, Cesium D Line Data, <http://steck.us/alkalidata> (2010).
- [32] A. Kramida, Y. Ralchenko, J. Reader, and NIST ASD Team, NIST Atomic Spectra Database, <https://physics.nist.gov/asd>.
- [33] R. Lin, D. Liu, J. Ruan, W. Zhao, and X. Wang, *Freq. Contr. Symp.* (2014).
- [34] F. Tricot, D. H. Phung, M. Lours, S. Guerandel, and E. de Clercq, *Rev. Sci. Instr.* **89**, 113112 (2018).